Supporting Information

Dual electron transfer path and LSPR photothermal enhancement in BiOCl@$ZnIn_2S_4$ heterojunction for enhanced photocatalytic H_2 evolution, H_2O_2 production and tetracycline removal

Fan Wu[a], Guangyu Wu [a, b*], Yonggong Tang[a], Yuwei Pan[a], Jiangang Han[c], Jin Zhang[d], Weinan Xing[a], Yudong Huang[e]

a. College of Ecology and Environment, Co-Innovation Center for the Sustainable Forestry in Southern China, Nanjing Forestry University, Nanjing 210037, China

b. Guangxi Key Laboratory of Petrochemical Resource Processing and Process Intensification Technology, School of Chemistry and Chemical Engineering, Guangxi University, Nanning 530004, China

c. School of Chemical Engineering and Materials, Changzhou Institute of Technology, Changzhou 213032, China

d. State Key Laboratory of Chemical Engineering, School of Chemical Engineering, East China University of Science and Technology, Shanghai 200237, China

e. MIIT Key Laboratory of Critical Materials Technology for New Energy Conversion and Storage, School of Chemistry and Chemical Engineering, Harbin Institute of Technology, Harbin, 150001, China

E-mail: gywuchem@njfu.edu.cn

Materials

All chemicals used in this experiment were analytically pure and required no further purification. $Bi(NO_3)_3•5H_2O$, $ZnCl_2$, L-histidine ($C_6H_9N_2O_2$, L-his), p-benzoquinone ($C_6H_4O_2$, BQ), Acetonitrile (C_2H_3N) and Triethanolamine ($C_6H_{15}NO_3$) were purchased from Shanghai Macklin Biochemical Co., Ltd. $[Ru(bpy)_3]Cl_2•6H_2O$ was purchased from Shanghai Aladdin Biochemical Technology Co., Ltd. EDTA, KCl and tert-butanol ($C_4H_{10}O$, TBA) were purchased from Sinopharm Chemical Reagent Co., Ltd. Ethylene glycol ($C_2H_6O_2$) was purchased from Nanjing Chemical Reagent Co., Ltd. Thanol (C_2H_5OH) was purchased from Shanghai Titan Scientific Co., Ltd. TC was purchased from Sun Chemical Technology (Shanghai) Co., Ltd. Thioacetamide (TAA) and $InCl_3•4H_2O$ were purchased from Shanghai Yien Chemical Technology Co., Ltd.

Characterization

The functional group information of the sample were observed through Fourier transform infrared spectroscopy (FT-IR, Bruker VERTEX 80V, Germany). The composition and crystal structure of the samples was identified by X-ray diffraction (XRD, Rigaku Ultima IV, Japan). The micro morphology and the internal fine structure of composite materials were obtained by scanning electron microscope (SEM, JEOL 7600F, Japan) and transmission electron microscope (TEM, JEOL JEM 2100, Japan). UV-Vis DRS (Shimadzu UV-3600) was used to evaluate the optical absorption characteristics and calculate the band gap. X-ray photoelectron spectroscopy (XPS, Thermo Fisher escalab 250xi, USA) was used to further understand the elemental

composition and valence information of materials. PL spectra were tested by FLS980 (Edinburgh, Britain). The separation effect and photoelectric properties of the photocatalyst were studied by photoluminescence spectroscopy, transient photocurrent response and electrochemical impedance spectroscopy (CHI-760E).

Photoelectrochemical test

Mott-Schottky experiments (M-S) were conducted on a CHI 760E electrochemical workstation with the universal three-electrode test system. In a 2 mL test tube, 5 mg of material, 1 mL of ethanol and 10 μL of nafion solution were added as dispersant and then sonicated for 2 min to form a homogeneous mixed solution. Subsequently, the working electrode was prepared by uniformly applying the mixed solution onto an indium tin oxide (ITO) glass conductive surface with an active area of 1 cm^2 , and dried at 60°C for 6 hours. A graphite electrode and Ag/AgCl electrode were used as the counter electrode and reference electrode, respectively. 0.5 M Na_2SO_4 solution was used as the electrolyte. The Mott-Schottky experiments were conducted at the frequency of 800, 1000 and 1200 Hz. The potential was calibrated by normal hydrogen electrode (NHE) and the formula was as the following:

$E_{NHE} = E_{Ag/AgCl} + 0.0592\ pH + 0.198\ eV$

Where E_{NHE} was the corrected potential vs. NHE, $E_{Ag/AgCl}$ was the measured potential vs. Ag/AgCl electrode, and pH was 6.8 at 25℃.

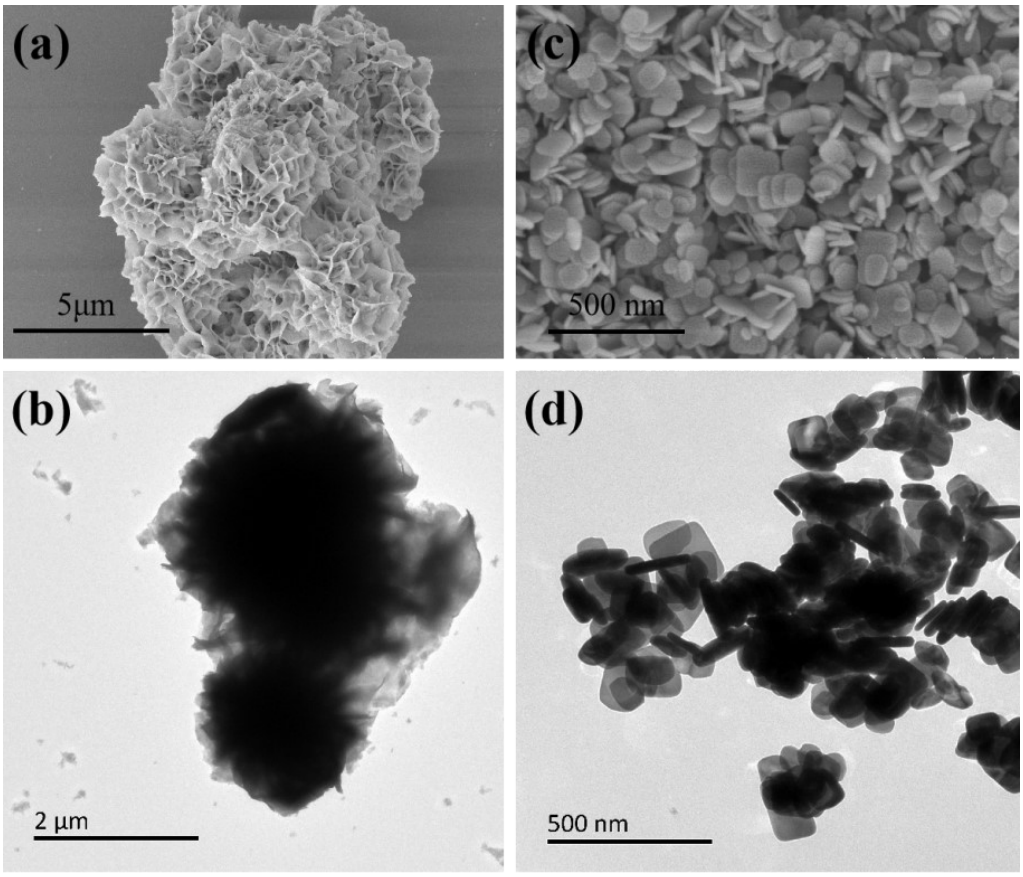

Fig. S1 SEM and TEM image of ZIS (a, b) and BiOCl (c, d).

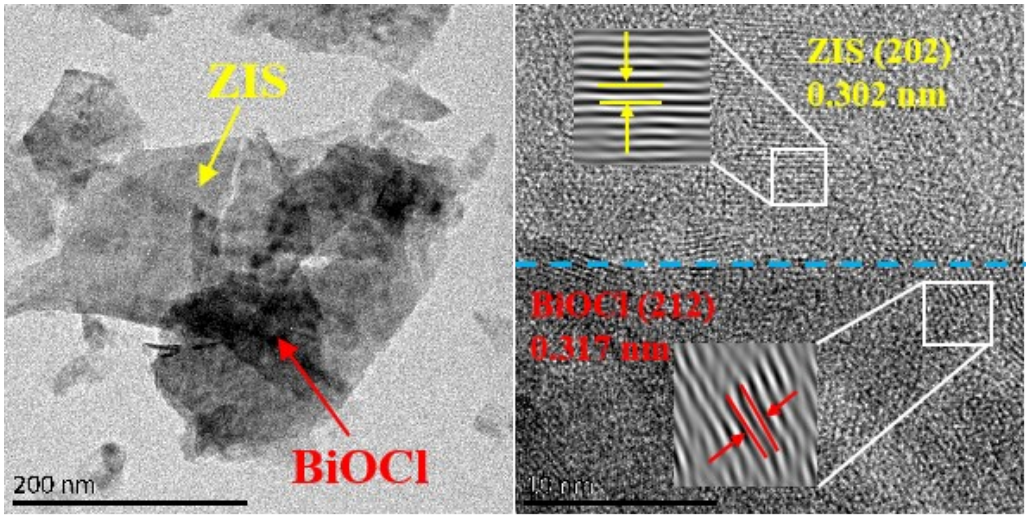

Fig. S2 HRTEN image of BiOCl@ZIS-1%.

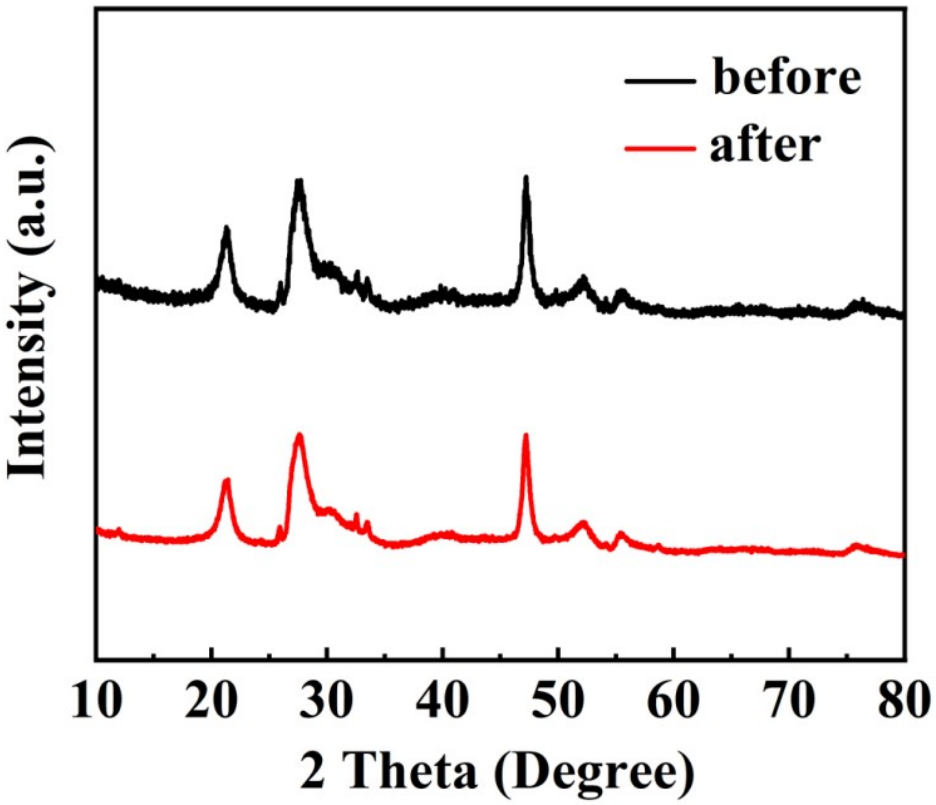

Fig. S3 XRD comparison of BiOCl@ZIS-1% before and after reaction.

Tab. S1 Comparison of H_2 generation with different catalysts of same conditions

Materials	Time (min)	H_2 generation	Reference
CoZnS@NSC-15/g-C_3N_4	240	610.8 μmol h^{-1} g^{-1}	1
NiSe/ZIS	150	3240.0 μmol h^{-1} g^{-1}	2
C@TiO_2	180	400.0 μmol h^{-1} g^{-1}	3
In_2O_3/In_2S_3-$CdIn_2S_4$	240	2892.0 μmol h^{-1} g^{-1}	4
ZIS/CN/ATP	180	3906.2 μmol h^{-1} g^{-1}	5
SnO_2/$BaSO_4$	240	5260 μmol h^{-1} g^{-1}	6
PBA/PTI-2	120	460.0 μmol h^{-1} g^{-1}	7
MO/C@ZIS	240	2357.0 μmol h^{-1} g^{-1}	8
CIS/CeO_2	180	226.6 μmol h^{-1} g^{-1}	9
BiOCl@ZIS-1%	240	13689.78 μmol h^{-1} g^{-1}	This work

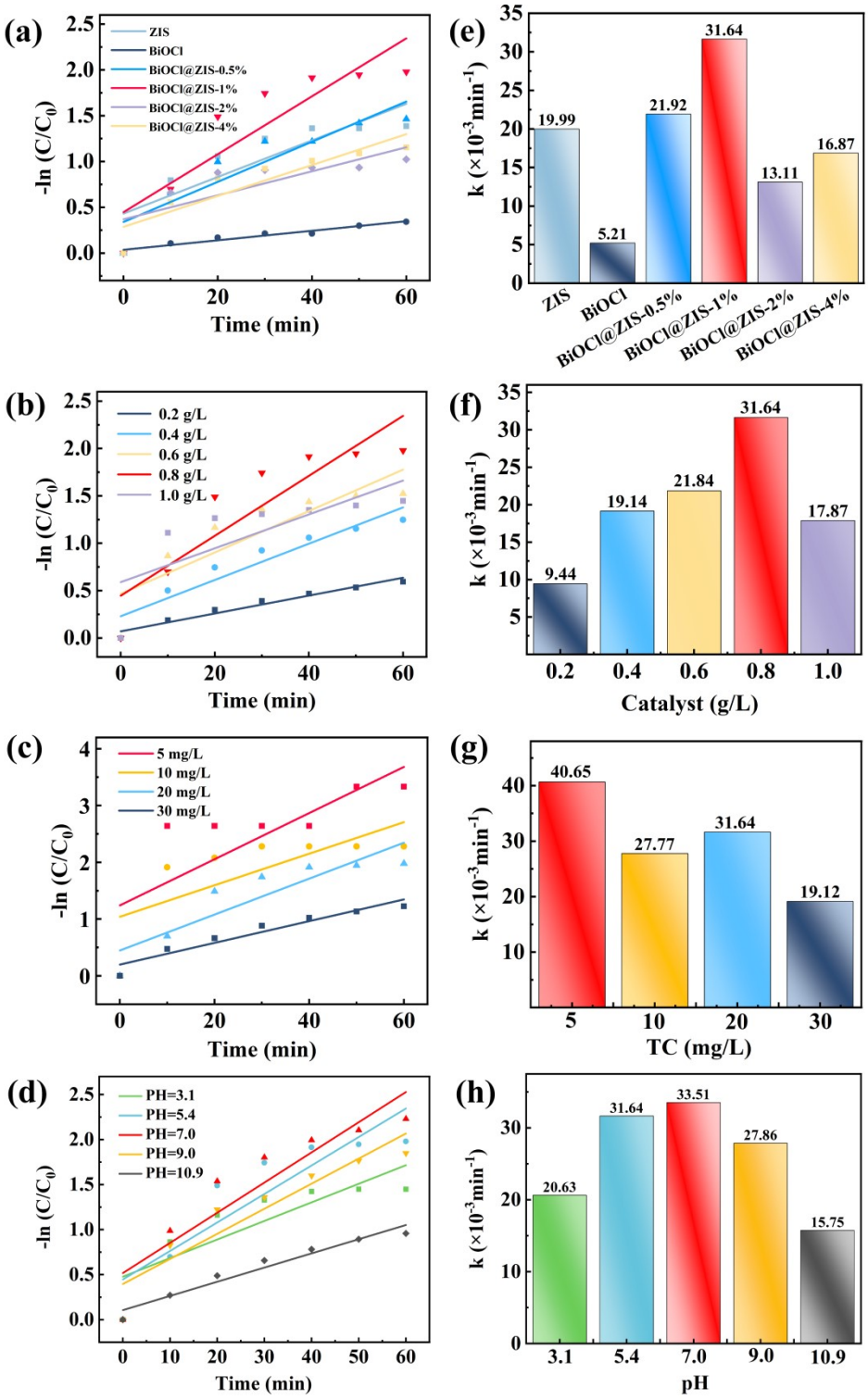

Fig. S4 Quasi-first-order kinetic equations and degradation rate constants of (a, e) different catalysts; (b, f) dosage; (c, g) TC concentration and (d, h) pH for TC degradation.

Tab. S2 Comparison of TC degradation with different catalysts

Materials	Degradation efficiency (%)	Time (min)	Reference
HOP	84.60	40	[10]
BWO-Ox	79.68	180	[11]
sp^2c-COF	73.50	90	[12]
CuO-NCP	67.00	300	[13]
CMCD-TiO@FeO@RGO	83.30	60	[14]
BFO/rGO	83.73	60	[15]
CuFeO/g-CN/rGO	67.00	150	[16]
Bi_2O_4@FeOOH	84.20	120	[17]
BiOI/$BiOIO_3$	75.90	270	[18]
AgCl/WO/g-CN	76.30	60	[19]
TiC-SOH/g-CN	75.42	120	[20]
BiOCl@ZIS-1%	86.00	60	This work

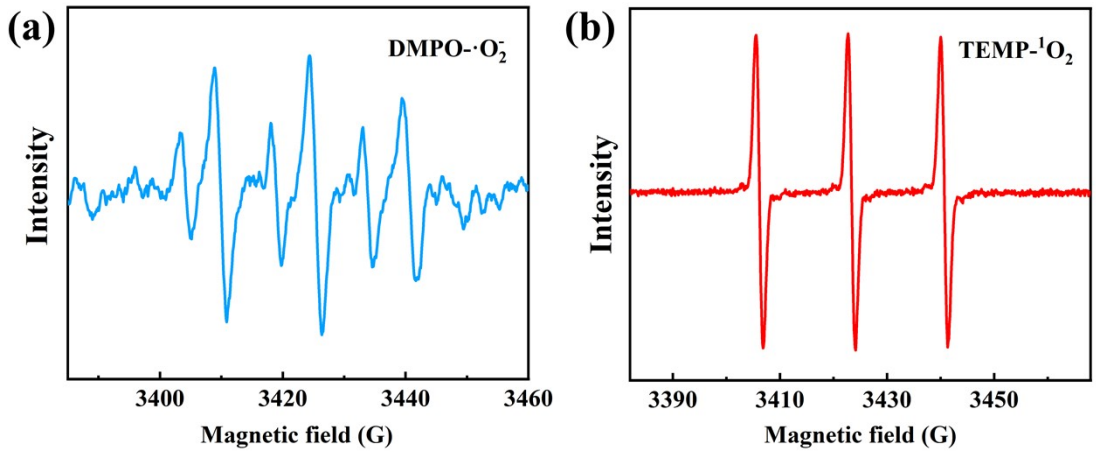

Fig. S5 EPR spectra of BiOCl@ZIS-1% in the presence of (a) DMPO and (b) TEMP.

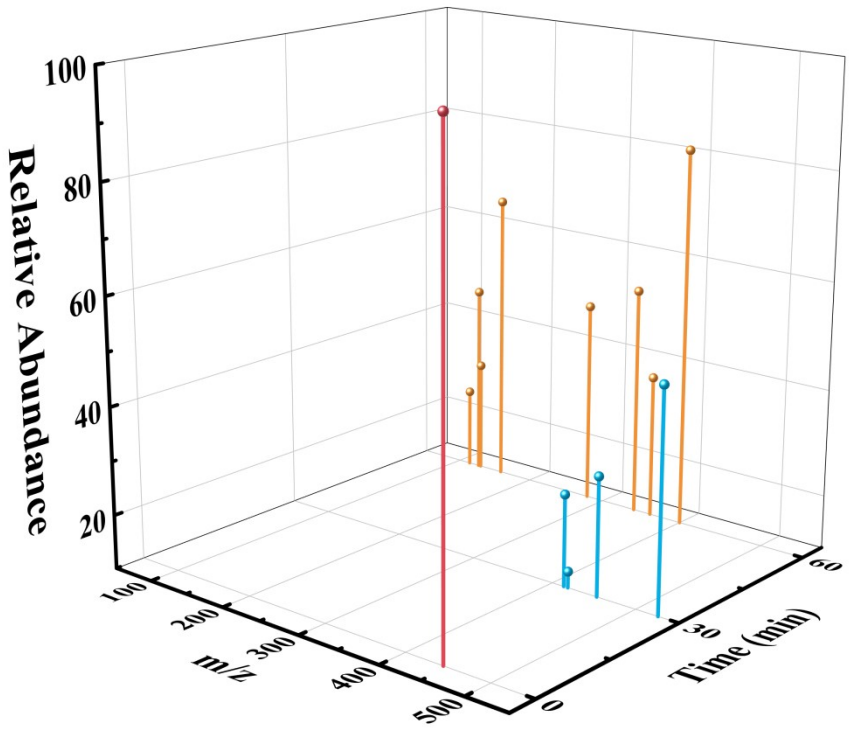

Fig. S6 Mass spectra of TC over BiOCl/ZIS-1% at 0 min, 30 min and 60 min.

Tab. S3 Comparison of H_2O_2 production with different catalysts in the same condition

Materials	Time (h)	Dosage (mg)	Solution volume (mL)	H_2O_2 production	Reference
BIO-OVs-2	2	50	50	4310 μM h^{-1} g^{-1}	[21]
Au(0.50)@MoS_2	12	50	50	1018.7 μM h^{-1} g^{-1}	[22]
BU-3	1	50	50	144.6 μM h^{-1} g^{-1}	[23]
g-C_3N_4-0.05	4	30	30	704.0 μM h^{-1} g^{-1}	[24]
$Au_{0.1}Ag_{0.2}/TiO_2$	24	5	5	2833.3 μM h^{-1} g^{-1}	[25]
Pt@β-CD/C_3N_4-M	1	60	60	147.1 μM h^{-1} g^{-1}	[26]
SCNx	2	10	50	8334 μM h^{-1} g^{-1}	[27]
BiOCl@ZIS-1%	120	10	50	9670 μM h^{-1} g^{-1}	This work

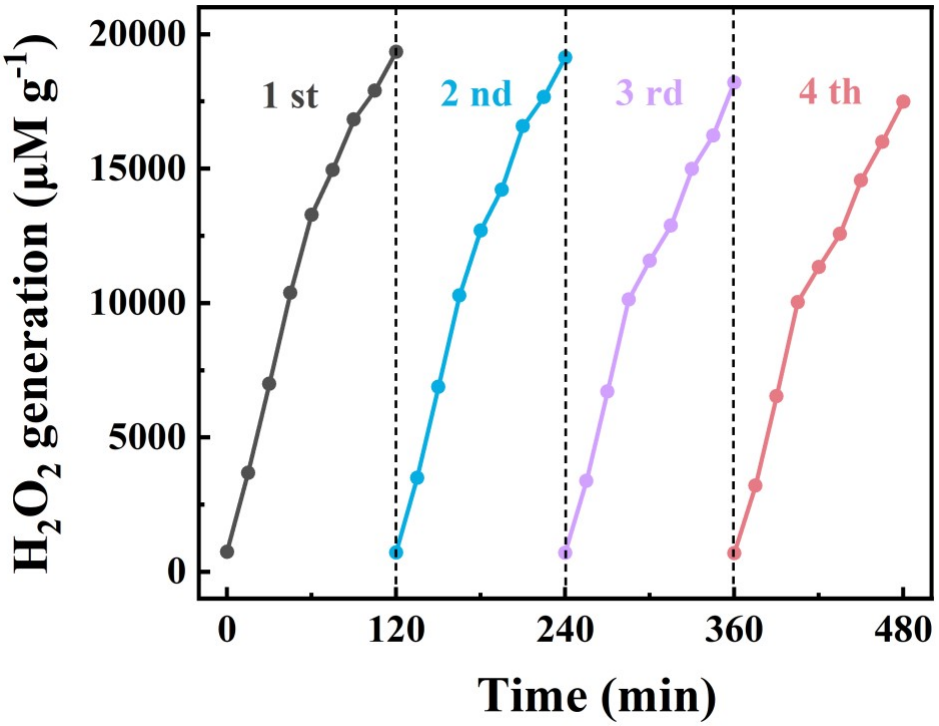

Fig. S7 Photocatalytic H_2O_2 production stability of BiOCl@ZIS-1%.

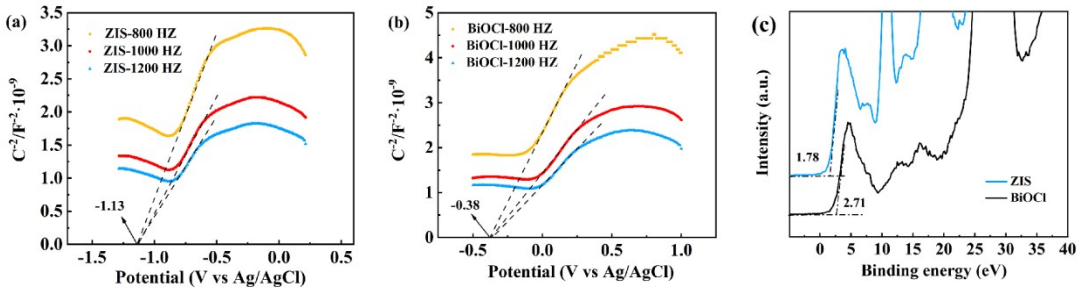

Fig. S8 (a, b) Mott-Schottky curves and (c) Valence bands (Ed) of BiOCl and ZIS.

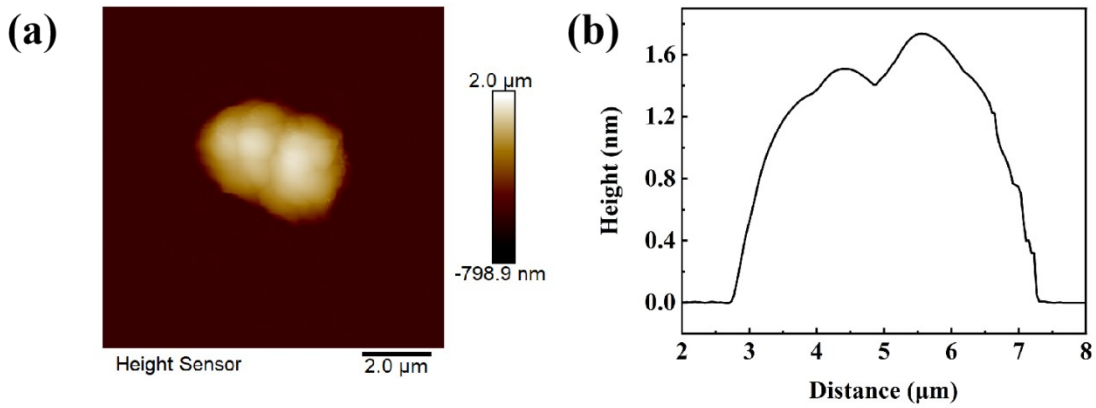

Fig. S9 AFM image of BiOCl@ZIS-1%.

Reference

1. X. J. Lu, I. Ullah, J. H. Li, S. Chen, C. Z. Yuan and A. W. Xu, A bimetallic CoZn metal-organic-framework derived CoZnS@NSC Co-catalyst loaded on gC_3N_4 for significantly augmented photocatalytic H_2 evolution, *Inorg. Chem. Front.*, 2024, **11**, 3435-3445.
2. S. Mansoor, Z. Hu, Y. Zheng, M. Tayyab, M. Khan, Z. Akmal, L. Zhou, J. Lei and J. Zhang, Comparative study of photocatalytic H_2 production by nickel chalcogenides$_{1+x}$ based $Zn_3In_2S_6$ photocatalytic system, *Sep. Purif. Technol.*, 2024, **353**, 128357.
3. Y. Deligiannakis, E. Bletsa, E. Mouzourakis, M. Solakidou and K. Adamska, Carbon-Coated TiO_2 Nanoparticles for Noble-Metal-Free Photocatalytic H_2 Production from H_2O, *ACS Appl. Nano Mater.*, 2024, **7**, 11621-11633.
4. Y. Qi, G. Zhou, Y. Wu, H. Wang, Z. Yan and Y. Wu, In-situ construction of In_2O_3/In_2S_3-$CdIn_2S_4$ Z-scheme heterojunction nanotubes for enhanced photocatalytic hydrogen production, *J. Colloid Interf. Sci.*, 2024, **664**, 107-116.
5. B. Wang, L. Huang, T. Peng, R. Wang, J. Jin, H. Wang, B. He and Y. Gong, Attapulgite-intercalated g-$C_3N_4/ZnIn_2S_4$ 3D hierarchical Z-scheme heterojunction for boosting photocatalytic hydrogen production, *J. Colloid Interf. Sci.*, 2024, **675**, 52-63.
6. C. Cheng, J. Zhang, H. Jia, X. Ding, G. Dong, F. Chen, Y. Hu and J. Shi, One-pot synthesis of amorphous/crystalline $SnO_2/BaSO_4$ composite sensitized with Eosin Y for enhanced photocatalytic H_2 production, *J. Environ. Chem. Eng.*,

2024, **12**, 112770.

7. Y. Ren, Y. Li, G. Pan, N. Wang, X. Liu and Z. Wu, A novel all-organic S-scheme heterojunction with rapid interfacial charges migration for efficient photocatalytic H_2 production, *J. Mater. Sci. Technol.*, 2024, **201**, 12-20.
8. X. Zhang, H. Ye, Z. Zeng, K. Sa, J. Jia, Z. Yang, S. Xu, C. Han and Y. Liang, Bridging the gap between metallic MoO_2 and $ZnIn_2S_4$ for enhanced photocatalytic H_2 production, *Sep. Purif. Technol.*, 2024, **347**, 127624.
9. J. Wang, X. Niu, Q. Hao, K. Zhang, X. Shi, L. Yang, H. Y. Yang, J. Ye and Y. Wu, Promoting charge separation in $CuInS_2/CeO_2$ photocatalysts by an S-scheme heterojunction for enhanced photocatalytic H_2 production, *Chem. Eng. J.*, 2024, **493**, 152534.
10. Y. Zhao, L. Chang, Y. Li, W. He, K. Liu, M. Cui, M. U. Hameed and J. Xie, High-gravity photocatalytic degradation of tetracycline hydrochloride under simulated sunlight, *J. Water Process Eng.*, 2023, **53**, 103753.
11. L. Chen, B. Xu, M. Jin, L. Chen, G. Yi, B. Xing, Y. Zhang, Y. Wu and Z. Li, Excellent photocatalysis of Bi_2WO_6 structured with oxygen vacancies in degradation of tetracycline, *J. Mol. Struct.*, 2023, **1278**, 134911.
12. Z. Hu, Y. Luo, L. Wang, Y. Wang, Q. Wang, G. Jiang, Q. Zhang and F. Cui, Synthesis of Pyrene-Based Covalent Organic Frameworks for Photocatalytic Tetracycline Degradation, *ACS Appl. Polym. Mater.*, 2023, **5**, 9263-9273.
13. M. Saberian and A. Nezamzadeh-Ejhieh, Synergistic photocatalytic degraded tetracycline upon supported CuO clinoptilolite nanoparticles, *Solid State Sci.*,

2024, **147**, 107381.

14. Z. Liu, G. Wang, Y. Li, H. Li and N. Deng, Carboxymethyl-β-cyclodextrin functionalized TiO_2@Fe_3O_4@RGO magnetic photocatalyst for efficient photocatalytic degradation of tetracycline under visible light irradiation, *J. Environ. Chem. Eng.*, 2024, **12**, 113303.

15. Z. Wu, J. Liu, J. Shi and H. Deng, $Bi_2Fe_4O_9$/rGO nanocomposite with visible light photocatalytic performance for tetracycline degradation, *Environ. Res.*, 2024, **249**, 118361.

16. R. Rajendran, O. Rojviroon, V. Vasudevan, P. Arumugam, M. Handayani, N. Akechatree, Y. Leelert and T. Rojviroon, Magnetically separable ternary heterostructure photocatalyst $CuFe_2O_4$/g-C_3N_4/rGO: Enhancing photocatalytic degradation and bacterial inactivation, *J. Water Process Eng.*, 2024, **63**, 105443.

17. Y. Sun, Y. Tang, F. Chen, P. Huang, W. Sun and Y. Song, Amorphous FeOOH shell decorated Bi_2O_4 for the boosted photocatalytic degradation of tetracycline under visible irradiation, *J. Environ. Chem. Eng.*, 2024, **12**, 112181.

18. W. Mu, L. Wang and C. Chang, Photocatalytic adsorption/degradation of tetracycline by S-scheme BiOI/$BiOIO_3$ pn heterojunction from dissociation of $BiOIO_3$ in-situ solvothermal process, *J. Environ. Manag.*, 2024, **356**, 120630.

19. S. Pu, Q. Zhao, X. Luo, D. Wang, K. Lei, Y. Duan, L. Mao, W. Feng and Y. Sun, In-situ synthesis of AgCl/WO_3 loaded with g-C_3N_4 as dual Z-scheme heterojunction for boosting photocatalytic degradation of antibiotics, *Surf.*

Interf., 2024, **46**, 104016.

20. J. Zhang, C. Shao, Z. Lei, Y. Li, H. Bai, L. Zhang, G. Ren and X. Wang, Treatment of antibiotics in water by SO_3H-modified Ti_3C_2 Mxene photocatalytic collaboration with g-C_3N_4, *J. Mater. Sci. Technol.*, 2024, **194**, 124-137.

21. A. Yuan, T. Huang, Y. Guo, Y. Wei, H. Liu, B. Yang and B. Chang, $BiOIO_3$ Nanoplates with Tailorable Surface Defects for Photocatalytic H_2O_2 Production, *ACS Appl. Nano Mater.*, 2024, **7**, 12761-12772.

22. H. Song, L. Wei, C. Chen, C. Wen and F. Han, Photocatalytic production of H2O2 and its in situ utilization over atomic-scale Au modified MoS2 nanosheets, *J. Catal.*, 2019, **376**, 198-208.

23. Y. Yang, C. Zhang, D. Huang, G. Zeng, J. Huang, C. Lai, C. Zhou, W. Wang, H. Guo and W. Xue, Boron nitride quantum dots decorated ultrathin porous g-C3N4: Intensified exciton dissociation and charge transfer for promoting visible-light-driven molecular oxygen activation, *Appl. Catal. B: Environ.*, 2019, **245**, 87-99.

24. H. Zhang, L. Jia, P. Wu, R. Xu, J. He and W. Jiang, Improved H_2O_2 photogeneration by KOH-doped g-C_3N_4 under visible light irradiation due to synergistic effect of N defects and K modification, *Appl. Surf. Sci.*, 2020, **527**, 146584.

25. D. Tsukamoto, A. Shiro, Y. Shiraishi, Y. Sugano, S. Ichikawa, S. Tanaka and T. Hirai, Photocatalytic H_2O_2 production from ethanol/O_2 system using TiO_2

loaded with Au-Ag bimetallic alloy nanoparticles, *ACS catal.*, 2012, **2**, 599-603.

26. H. Zhu, Q. Xue, G. Zhu, Y. Liu, X. Dou and X. Yuan, Decorating Pt@cyclodextrin nanoclusters on C_3N_4/MXene for boosting the photocatalytic H_2O_2 production, *J. Mater. Chem. A.*, 2021, **9**, 6872-6880.

27. Y. Li, W. Wang, Y. Wang, H. He, X. Yu, D. Xia, L. Deng and Y.-N. Liu, Edge engineering of carbon nitride for enhanced sacrificial agent-free photocatalytic H_2O_2 evolution, *Chem. Eng. Sci.*, 2023, **282**, 119333.